JGR Space Physics

RESEARCH ARTICLE
10.1029/2023JA031430

Interhemispheric Asymmetry Due To IMF By Within the Cusp Spherical Elementary Currents

J. M. Weygand[1], M. D. Hartinger[2], R. J. Strangeway[1], D. T. Welling[3], Hyomin Kim[4], Jürgen Matzka[5], and C. Robert Clauer[6]

[1]Department of Earth Planetary, and Space Science, University of California Los Angeles, Los Angeles, CA, USA, [2]Space Science Institute, Boulder, CO, USA, [3]Department of Atmospheric, Oceanic, and Space Sciences, University of Michigan, Ann Arbor, MI, USA, [4]New Jersey Institute of Technology, Newark, NJ, USA, [5]GFZ German Research Centre for Geosciences, Potsdam, Germany, [6]Virginia Tech, Blacksburg, VA, USA

Key Points:

- We show the instantaneous equivalent ionospheric current orientation in the cusp for positive and negative IMF By
- We demonstrate that this pattern is reversed in opposite hemispheres
- Magnetically conjugate spherical elementary currents provide an opportunity to observe the high temporal variation in the cusp region

Supporting Information:

Supporting Information may be found in the online version of this article.

Correspondence to:

J. M. Weygand,
jweygand@igpp.ucla.edu

Citation:

Weygand, J. M., Hartinger, M. D., Strangeway, R. J., Welling, D. T., Kim, H., Matzka, J., & Clauer, C. R. (2023). Interhemispheric asymmetry due to IMF By within the cusp spherical elementary currents. *Journal of Geophysical Research: Space Physics*, *128*, e2023JA031430. https://doi.org/10.1029/2023JA031430

Received 22 FEB 2023
Accepted 20 MAY 2023

Author Contributions:

Conceptualization: J. M. Weygand, D. T. Welling
Data curation: J. M. Weygand, D. T. Welling, Hyomin Kim, Jürgen Matzka, C. Robert Clauer
Formal analysis: J. M. Weygand, R. J. Strangeway, D. T. Welling, Hyomin Kim
Funding acquisition: M. D. Hartinger, D. T. Welling
Investigation: J. M. Weygand, D. T. Welling
Methodology: J. M. Weygand
Project Administration: M. D. Hartinger
Supervision: M. D. Hartinger, R. J. Strangeway
Validation: R. J. Strangeway
Visualization: J. M. Weygand
Writing – original draft: J. M. Weygand

Abstract Observations of interhemispheric asymmetry in the cusp region due to the interplanetary magnetic field (IMF) By component have been performed for years, but those observations typically are not simultaneous in both hemispheres and represent an average picture. Simultaneous instantaneous observations in both hemispheres are rare. We have combined four sets of magnetometers in Antarctica to produce equivalent ionospheric currents and current amplitudes at 10 s resolution using the spherical elementary current systems technique. These Antarctica spherical elementary currents are roughly conjugate to the northern hemisphere spherical elementary currents derived over Greenland and North America. We examined five intervals with large interplanetary magnetic field By positive and negative and demonstrate that the equivalent current pattern in opposite hemispheres are asymmetric with respect to one another during IMF By positive with the cusp throat opening towards the dusk in the northern hemisphere and towards the dawn in the southern hemisphere. This configuration reverses for interplanetary magnetic field By negative. In one of these events we examine the rotation of the equivalent currents in real time in the northern hemisphere. We also compare these results with virtual magnetometer predictions from the Space Weather Modeling Framework. Simultaneous spherical elementary currents observations in both hemispheres are important because they allow us to observe the evolution of the cusp throat during changing solar wind and interplanetary magnetic field conditions.

1. Introduction

The classical picture of the Dungey cycle (Dungey, 1961) shows that during southward interplanetary magnetic field (IMF) the IMF reconnects with the magnetosphere and convects across the polar cap where the reconnection at the magnetopause is an arc along the dayside magnetopause near the magnetic equatorial plane at noon and the throat of cusp opens towards noon (Cowley & Owen, 1989; Crooker, 1979). When IMF By component is positive or negative the reconnection line can become twisted (Crooker, 1979; Trattner et al., 2007a, 2007b, 2012, 2021), the throat of cusp may no longer open towards noon (Crooker, 1979; de La Beaujardiere et al., 1993), and the throat points in opposite direction in opposite hemispheres (Burch et al., 1985; Cowley, 1981; Cowley et al., 1991; Reiff & Burch, 1985).

Specifically, the throat of cusp opens towards the dusk in the northern hemisphere for IMF By positive and towards the dawn for IMF By negative (Burch et al., 1985; Cowley et al., 1991; Reiff & Burch, 1985; Strangeway et al., 2000). The throat of cusp has the opposite arrangement in the southern hemisphere (Strangeway et al., 2021; and implied by Burch et al. (1985) and Reiff and Burch (1985)). Figure 1 displays the configuration of the cusp throat for both hemispheres, which has the equivalent ionospheric currents drawn as the black curves, for IMF By positive on the top and negative on the bottom. This figure has been adapted from Strangeway et al. (2021). The configuration of the field aligned like currents shown in Figure 1 and the ionospheric flows has been statistically shown with the Active Magnetosphere and Planetary Electrodynamics Response Experiment (AMPERE) current densities and the SuperDARN radar data (Anderson et al., 2008, 2018; Thomas & Shepherd, 2018).

We have shown that several studies have examined the statistical and specific event configurations of the field aligned like currents and ionospheric flow patterns for a range of IMF By directions and several studies have examined the arrangement of field aligned like currents and ionospheric flow patterns in both hemisphere as a function of IMF By. However, no studies, as far as we are aware, have looked at the simultaneous equivalent ionospheric current patterns that require no integration time to be derived in both hemispheres. The equivalent

Writing – review & editing: J. M. Weygand, M. D. Hartinger, R. J. Strangeway, Hyomin Kim, Jürgen Matzka, C. Robert Clauer

ionospheric currents are the combination of both the Hall current and the Pedersen currents in a non-uniform conducting ionosphere, but, in general, the bulk of the equivalent ionospheric currents are the Hall currents. The Hall currents are, by definition, antiparallel to the ionospheric flow. Based on this argument the equivalent ionospheric currents can provide a general picture of the ionospheric flow pattern (Benkevitch et al., 2006; Weygand et al., 2012). In this study, we employ the spherical elementary current systems (SECS) method to produce the equivalent ionospheric currents, which are instantaneous maps of the ionospheric currents that could be used to study the real time development of the cusp throat region during changing IMF By conditions.

In the next section, we briefly discuss the different data sets to be used in this study. In the observation section, we show the observations for five events for various non-zero directions of the IMF By. Finally, we discuss our findings and summarize the results.

2. Data

The data for this study come from four sources: 11 different arrays of ground magnetometers covering North America and Greenland, 4 different arrays of ground magnetometer sources covering a region of Antarctica, AMPERE, and results from the Space Weather Modeling Frame Work (SWMF) for 8 October 2012.

Ground-based magnetometer data for the SECs comes from 11 distinct arrays across North America and Greenland. The left side of Figure 2 shows the distribution of these stations. These arrays include AUTUMN (Athabasca University THEMIS UCLA Magnetometer Network, NRCan (Natural Resources Canada), MACCS (Magnetometer Array for Cusp and Cleft Studies) (Engebretson et al., 1995) CARISMA (Canadian Array for Real time Investigations of Magnetic Activity) (Mann et al., 2008), GIMA (Geophysical Institute Magnetometer Array), Technical University of Denmark (DTU) Magnetometer Ground Stations in Greenland, McMAC (Mid-continent MAgnetoseismic Chain) (Chi et al., 2013), THEMIS GMAG (Ground MAGnetometers) (Russell et al., 2008), USGS (United States Geophysical Survey), the Falcon array, and the STEP (Solar-Terrestrial Energy Program) magnetometer array. In this study, we employ the SECS technique developed by Amm and Viljanen (1999), which uses the horizontal components of magnetometer data from an array of ground stations to infer ionospheric equivalent vector currents. The magnetometer data from these arrays are used to produce a two-dimensional map of ionospheric currents over North America and Greenland. Amm and Viljanen (1999), Weygand (2009a, 2009b), Weygand et al. (2011), and Weygand and Wing (2016) provide more details on the description of the SECS technique over Greenland and North America and the calculation of the spherical elementary currents (SECs). The number of available magnetometer stations for each two-dimensional map of ionospheric currents typically changes from day-to-day due to data gaps, changes in baseline, and measurement errors. One feature of this data set relevant to this study is these ionospheric currents require no integration time and they are essentially an instantaneous map of the ionospheric currents.

During a period from about 2015 to 2016 a limited region of Antarctica, which is magnetically conjugate to western Greenland, is covered with magnetometers from 4 different sources. The right side of Figure 2 shows the distribution of these stations. These sources include the Virginia Tech magnetometer array (Clauer et al., 2014), the British Antarctica Survey low power magnetometer network, the New Jersey Institute of Technology magnetometer array (Melville et al., 2014; Mende et al., 2009), and the German geomagnetic observatory Neumayer Station III (VNA, operated by Alfred-Wegener-Institute for Polar and Marine Research and the GFZ German Research Centre for Geosiences) (Matzka, 2016; Wesche et al., 2016), which is part of the global INTERMAGNET network and produces 1 Hz calibrated geomagnetic data. Similar to the North American region we produce two dimensional maps of the SECs over part of Antarctica. The spatial resolution of the equivalent ionospheric currents are 3° GLat and 7° GLong and the temporal resolution is 10 s. The spatial resolution was selected to make the comparison between the northern and southern hemispheres as close as possible, however, the density of magnetometers in the densest location is similar to the densest region in North America.

The AMPERE project uses the magnetic field data from the 66 iridium spacecraft at about 800 km in altitude in 6 different orbital planes to calculate the magnetic field perturbations and from those perturbations the current densities in the polar region with a latitudinal resolution of about 1°, a longitudinal resolution of about 30°, and a temporal resolution of a few minutes. However, each two dimensional picture of the currents requires 10 min of magnetometer data within the auroral region. The AMPERE project uses spherical harmonic analysis to obtain the current densities (Anderson et al., 2000; Waters et al., 2001).

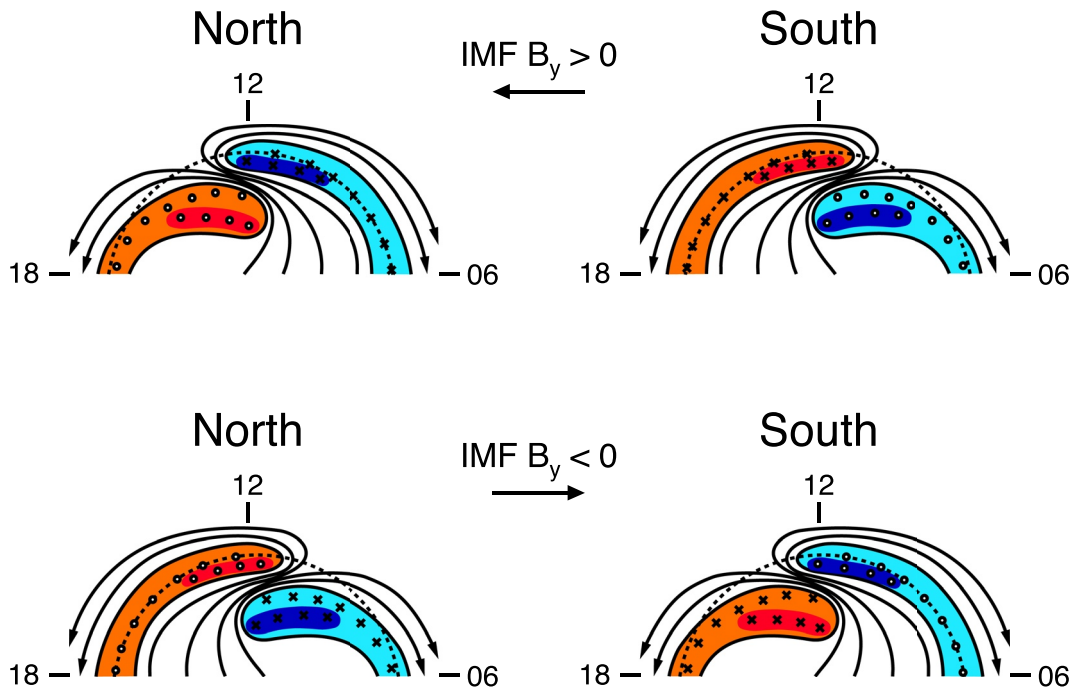

Figure 1. Ionospheric field aligned current and equivalent ionospheric current (black curves with arrows) configurations for the IMF By positive (top row) and negative (bottom row). The coordinate system is a magnetic coordinate system. Red areas indicates current out of the ionosphere and blue areas indicates current into the ionosphere. The southern hemisphere is shown as a glass earth configuration.

3. Observations

In this section, we will examine five different events: 17 March 2015, 5 June 2015, 20 March 2016, 28 July 2016, and 8 October 2012 when we have simultaneous northern hemisphere and southern hemisphere equivalent ionospheric current observations, AMPERE current densities, or Space Weather Modeling Framework (SWMF) results.

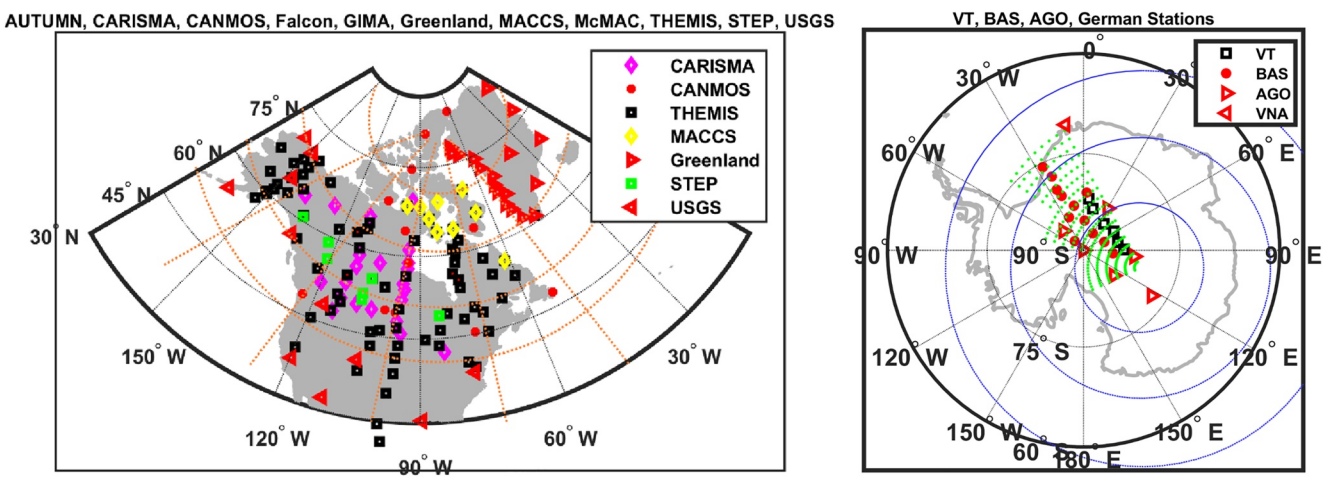

Figure 2. The left panel shows the ground magnetometers stations over North America and Greenland potentially contributing data to the SEC maps. The black lines are geographic coordinates and the orange lines are the magnetic coordinate system. The legend indicating the source of the magnetometer data is in the upper right corner in both panels. The right panel shows southern hemisphere ground magnetometers potentially contributing to the southern SEC maps. The mauve circles are the magnetic latitudes.

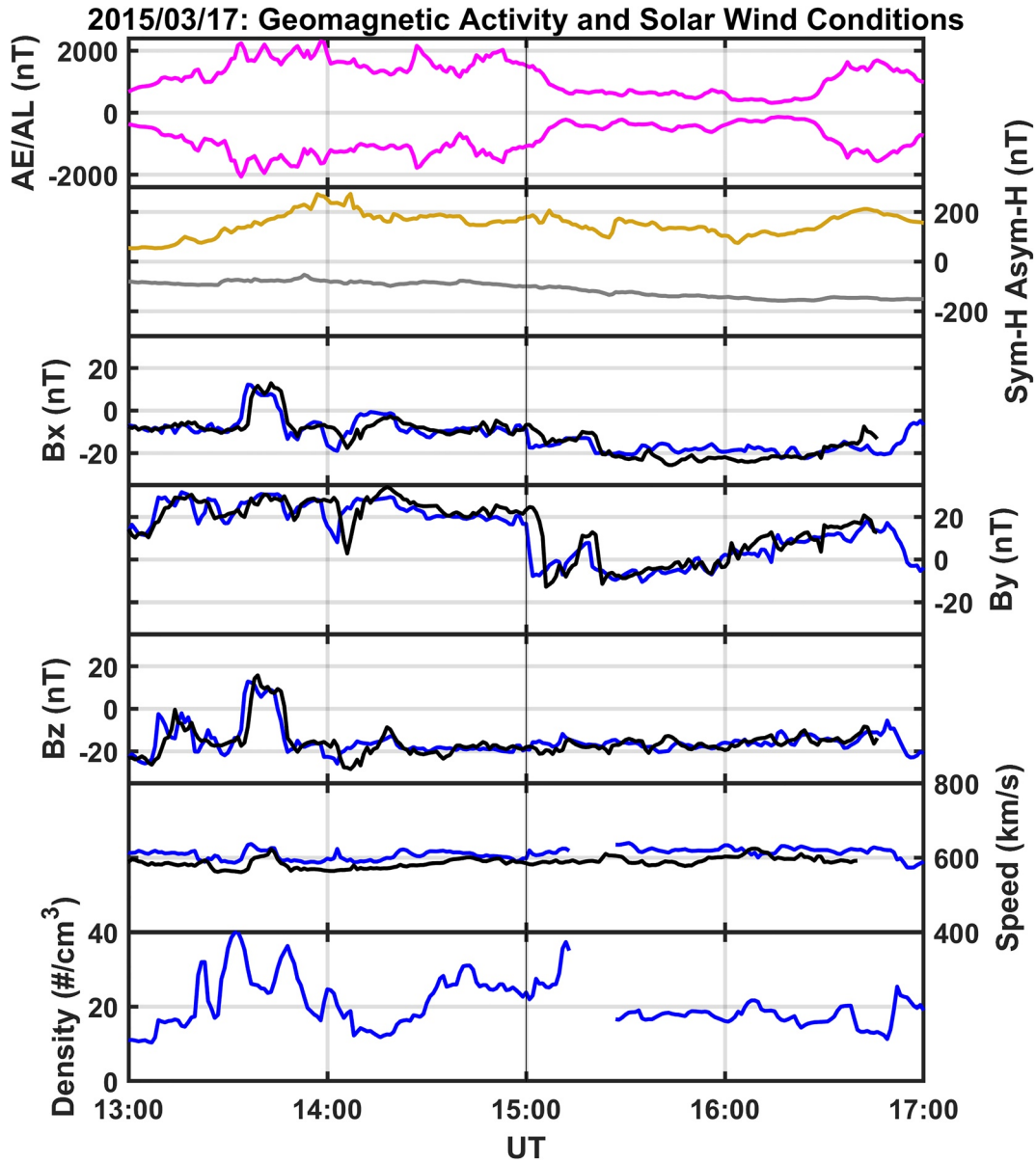

Figure 3. Geomagnetic and solar wind conditions for 17 March 2015. The top panel shows the World Data Center AE and AL indices, the second panel gives the Asym-H (orange) and Sym-H (gray) indices, the next three panels provide the ACE (black) and Wind (blue) propagated IMF Bx, By, and Bz components, the sixth panel displays the ACE and Wind propagated solar wind speed, and the bottom panel shows the Wind propagated solar wind density.

3.1. 17 March 2015: IMF By > 0 nT Event

Figure 3 shows the geomagnetic and solar wind conditions surrounding the period of interest at 1500 UT during the March 2015 magnetic storm, which begins at about 12 UT on 17 March 2015 to about 18 UT on 19 March 2015. The top panel demonstrates that this is a geomagnetically active period with the AL index (lower mauve curve) on the order of −1,000 nT for the hour before 1500 UT. The Sym-H index shown in the second panel demonstrates this event is a magnetic storm period. The next three panels display the ACE (blue) and Wind (black) propagated IMF components. The IMF data has been propagated using the Weimer et al. (2003) and Weimer (2004) technique to a fixed position (17, 0, 0) Re GSM. The bottom two panels show the ACE and Wind propagated solar wind speed and density. The two most important features of this figure are a period of about 2 hr of IMF By > 0 nT from about 13 to 15 UT and the approximate 70 min of Bz < 0 nT from about 1350 UT to 1500 UT. These observation suggested that the magnetic reconnection should occur and the cusp throat should open

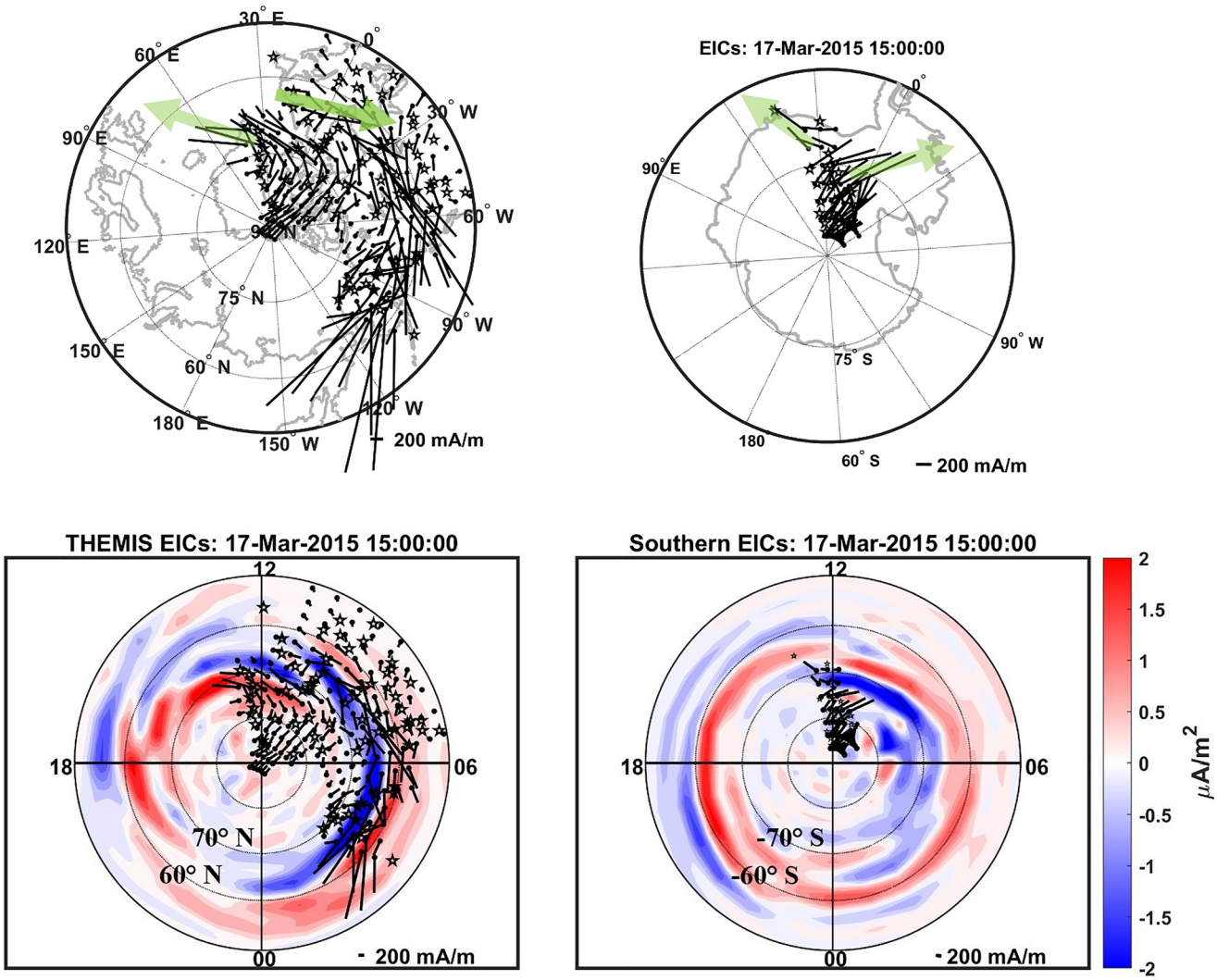

Figure 4. Northern and southern hemisphere equivalent ionospheric currents and AMPERE current densities for 15 UT on 17 March 2015 shown in a magnetic coordinate system with noon at the top of the panel, midnight at the bottom of the panel, dusk on the left side, and dawn on the right side. The southern hemisphere is shown as a glass earth projection. The top row shows the equivalent ionospheric currents where the dot indicates the position at which the current is determined and the vectors indicates the magnitude and direction of the current. The green arrows point in the approximate direction of the equivalent current. The key is in the lower right corner of the plot. The bottom row displays the AMPERE current densities with the equivalent currents overlain on the AMPERE data.

towards the dusk in the northern hemisphere and towards the dawn in the southern hemisphere. In fact, Figure 3 of Xu et al. (2017) clearly shows during this period considerable interhemispheric asymmetry exists within the Bx component of the ground magnetometer data between the near conjugate ground magnetometers located in western Greenland and the Virginia Tech magnetometer array in central Antarctic from about 1130 to 1530 UT.

Figure 4 displays the equivalent ionospheric currents determined using the SECS method at 1500 UT in a magnetic coordinate system and the AMPERE current densities for both the northern and southern hemisphere. The southern hemisphere is shown as a glass earth projection such that both hemispheres have magnetic noon at the top of the panel, midnight at the bottom, dusk on the left side, and dawn on the right side. The range of magnetic latitude (MLat) in the upper left is from 50° MLat to 90° MLat, but only from −60° to −90° MLat in the upper right panel due to the limited number of southern hemisphere stations. In the upper left panel at about 70° MLat in the noon meridian the equivalent currents point toward the dusk as indicated by the high latitude green arrow, which indicates ionospheric flow from the dusk into the polar cap. Both Benkevitch et al. (2006) and Weygand et al. (2011) have previously demonstrated that the magnetic equivalent convection and equivalent ionospheric currents, which are for the most part the Hall currents, are roughly antiparallel to the ionospheric

flow. From about 0° to about 90° west magnetic longitude (WMLong) at 60° MLat the equivalent currents flow from the dawnside toward the dusk side as indicated by the low latitude green arrow, which indicates east to west ionospheric flow. This arrangement of the equivalent ionospheric currents is antiparallel to the flows shown in Figure 3a of Cowley et al. (1991). In the upper right panel of Figure 4 the arrangement of the equivalent currents in the southern hemisphere is opposite that of the northern hemisphere, which indicates that the cusp throat opens towards the dawn.

The bottom row of Figure 4 shows the field aligned AMPERE current densities for both the northern (lower left) and southern (lower right) hemisphere with the equivalent ionospheric currents overlain on the current densities. The color bar for the current densities is in the far right corner and red indicates upward current out of the ionosphere and blue indicates current into the ionosphere. The arrangement of the current densities for IMF By > 0 for the northern hemisphere is similar to Figure 5e of Anderson et al. (2008), which indicates the cusp opens towards the dusk in the northern hemisphere. The lower right panel for the southern hemisphere has nearly opposite arrangement of the field aligned like current densities and indicates the cusp opens towards the dawn. Both the northern and southern hemisphere equivalent currents and AMPERE radial currents have a similar configuration as the top row of Figure 1.

3.2. 5 June 2015: IMF By < 0 nT Event

Figure 5 shows the geomagnetic and solar wind conditions surrounding the period of interest that begins at 13 UT and lasts to 17 UT on 5 June 2016. This figure has the same format as Figure 3. The top panel demonstrates that this is a geomagnetically active period with the AL index (lower mauve curve) on the order of −800 nT for the hour before 1500 UT. The Sym-H index in the second panel shows this event is not a magnetic storm period. The IMF Bx component in the third panel rotates from about −10 nT at 14 UT to about +13 nT by 15 UT. The By component decreases from about 0 nT at 1345 UT to −17 nT by 1510 UT and the Bz component increase from about −13 nT at 14 UT to 0 nT by 15 UT and then back down to about −13 nT by 1530 UT. These observations suggested that magnetic reconnection should occur and the cusp should open towards the dawn in the northern hemisphere and towards the dusk in the southern hemisphere.

Figure 6 displays the equivalent ionospheric currents determined using the SECS method at 1500 UT and the AMPERE current densities for both the northern and southern hemisphere with the same format as Figure 4 during IMF By < 0. In the upper row of Figure 6 the arrangement of the equivalent currents in the southern hemisphere is opposite that of the northern hemisphere and indicates that the cusp throat opens towards the dawn in the north. Furthermore, the arrangement of the equivalent currents for IMF By < 0 is the reverse pattern of those shown in Figure 4 for IMF By > 0. The bottom row of Figure 6 displays the field aligned like AMPERE current densities for both the northern and southern hemispheres with the equivalent ionospheric currents overlain on the current densities. The arrangement of the current densities for IMF By < 0 for the northern hemisphere is similar to Figure 5w of Anderson et al. (2008), which indicates the cusp opens towards the dawn in the northern hemisphere. The lower right panel for the southern hemisphere has nearly opposite arrangement of the field aligned like current densities and indicates the cusp opens towards the dusk. Both the northern and southern hemisphere equivalent currents and AMPERE radial currents have a similar configuration as the bottom row of Figure 1.

3.3. 20 March 2016: IMF By < 0 nT to By > 0 nT

In the last two events we examined the rotation of the equivalent currents in the northern and southern hemisphere with changes in IMF By. On 20 March 2016 the IMF By rotates from mainly negative (before 1509 UT) with a value of about −3 nT to positive (after 1515 UT) with a value of about 2 nT while North America is in the noon sector. See Figure 7, which has the same format as Figures 3 and 5, but for this event Geotail data (red curves) is available and located at (23.2, 10.3, −1.0) Re GSM. During this rotation the AE index increases from about 100 to about 300 nT, but the Sym-H index stays relatively constant. The IMF Bz remains negative throughout the entire period, the Bx component decreases from about 4 nT to about 0 nT, and the solar wind speed is between 400 and 460 km/s. The number density provide by the Geotail low energy particle (LEP) instrument is significantly lower than Wind. The LEP instrument was designed for magnetospheric plasma observations and most likely did not have the ideal pointing direction to make solar wind number density measurements. Figure 8 displays three different times of the equivalent ionospheric currents during the IMF By rotation with the same format as

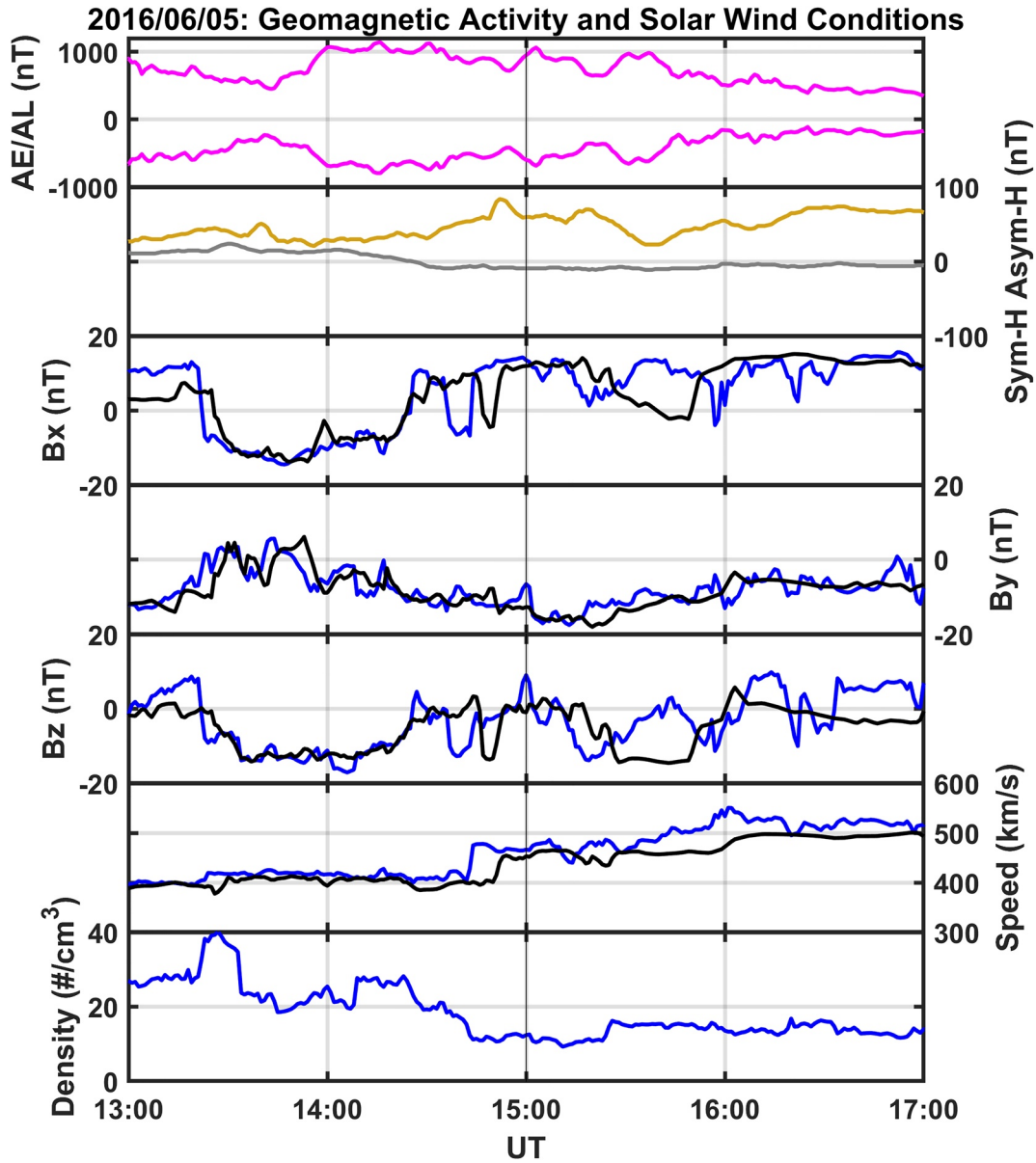

Figure 5. Geomagnetic and solar wind conditions for 5 June 2016. This figure has the same format as Figure 3. The time of interest in this figure is marked by a vertical gray line at 1500 UT.

the top panels of Figures 4 and 6. In each panel at about 70° MLat in the noon meridian we have indicated the approximate pointing direction of the cusp throat with the high latitude green arrow. At 14:56 UT in the top row of Figure 8 when IMF By < 0 the cusp throat points toward the dawn in the northern hemisphere and towards the dusk in the southern hemisphere. At 15:13 UT in the center row about 4 min after the By rotation in the solar wind the cusp throat roughly points towards magnetic noon. Then by 15:28 UT in the bottom row of Figure 8 about 19 min after the rotation of IMF By the rotation is complete and the cusp throat points toward the dusk in the northern hemisphere and towards the dawn in the southern hemisphere.

3.4. 28 July 2016: IMF By > 0 nT to By < 0 nT

On 28 July 2016 the IMF By sharply rotates from positive (before 1755 UT) to negative (after 1805 UT) at about 1800 UT while North America is in the dayside sector. See Figure 9 which has the same format as Figures 3 and 5. This gives us a second opportunity to watch the equivalent currents switch from one orientation to opposite

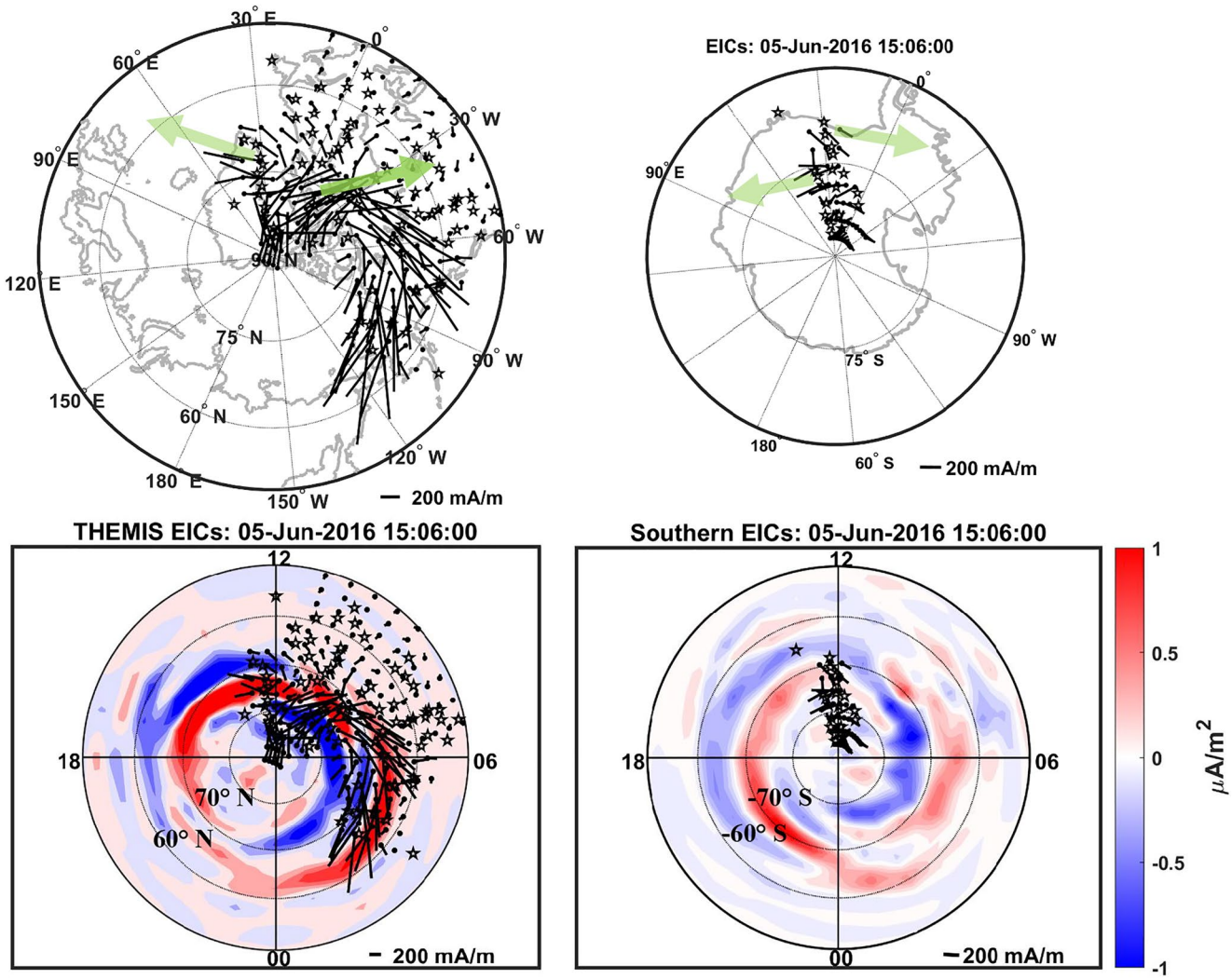

Figure 6. Northern and southern hemisphere equivalent ionospheric currents and AMPERE current densities for 15 UT on 5 June 2016.

orientation in the Northern Hemisphere. This event is unique because equivalent ionospheric currents rotate at different times with different latitudes. Unfortunately, the southern hemisphere magnetometers are not in the ideal position to see the change in the orientation of the currents. Figure 10 provides three SEC current maps before and after the rotation of the IMF By component. These maps are the combined equivalent ionospheric currents and the current density derived from the current amplitudes. The current amplitudes are converted into current densities by dividing the current by the rectangular area around the position of the current amplitude. In each panel, the currents are plotted across North America and Greenland on a geographic coordinate system. The vertical yellow bar marks local geographic midnight, and the color bar for the current density is given at the bottom of the figure. In the top panel at 0746 UT the equivalent ionospheric currents during IMF By > 0 nT at local noon point towards the east (dusk) and there is an unbroken band of downward current extending from northern Alaska to southern Greenland. The upward current are bifurcated within this map. In the middle panel at 1825 UT 20 min after the IMF By has completed the rotation to about −7 nT we see the first UT time the upward currents form an uninterrupted band of upward current from central Alaska to southern Greenland (marked with the orange dashed curve) and now the downward currents are bifurcated. The equivalent currents at local noon have formed and "S" shaped pattern at about 67 Glat and 90 WGlong where the lower latitude currents at about 64.8° GLat are pointing to the west (dawn) and the high latitude currents are pointing toward the east (dusk) at about 70.6° GLat. In the bottom panel at 1837 UT now all the currents at local noon are pointing westward (towards dawn) and the rotation of the equivalent currents is complete. A movie of the rotation of the equivalent current can be found in Movie S1.

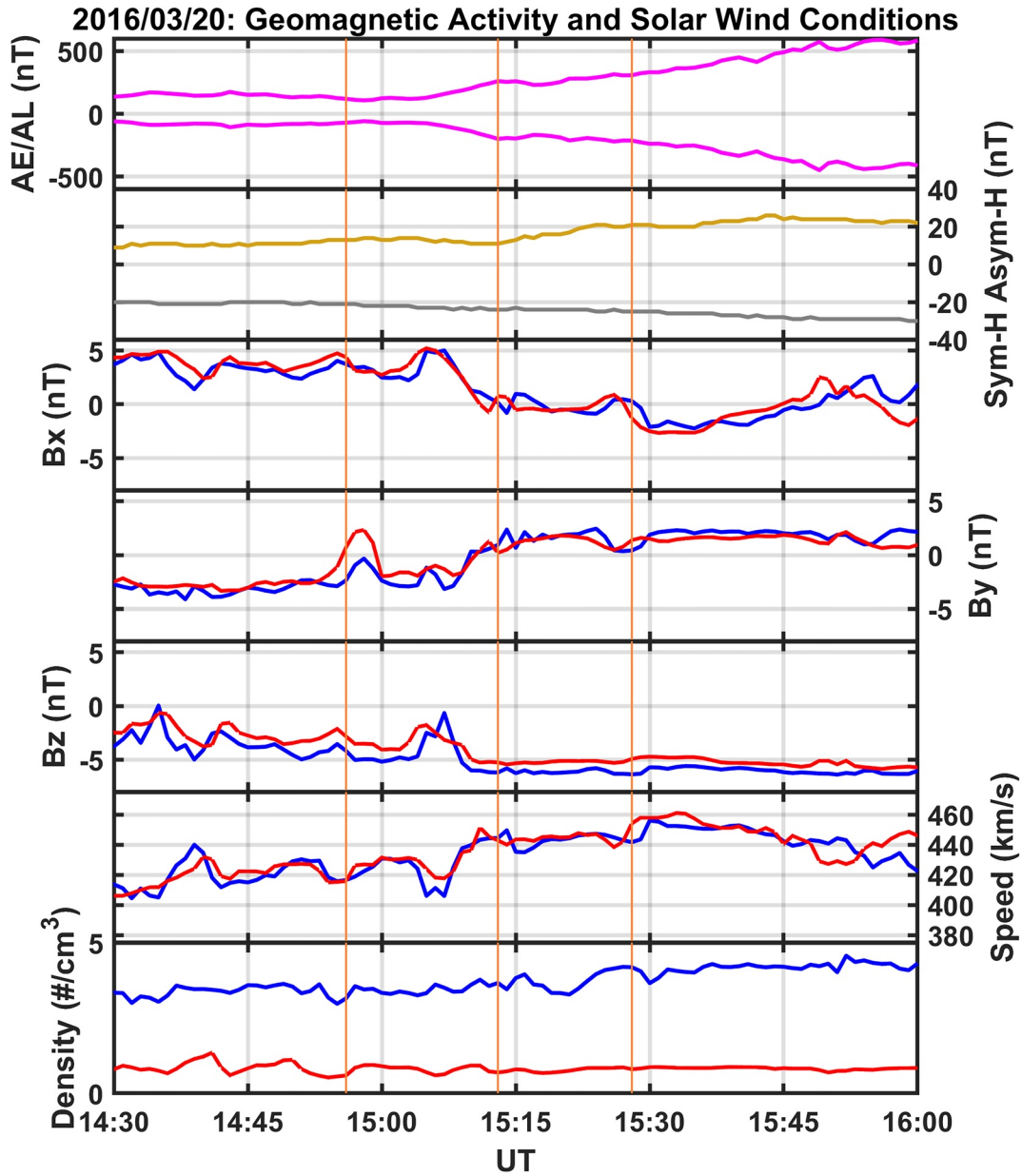

Figure 7. Geomagnetic and solar wind conditions for 20 March 2016. This figure has the same format as Figures 3 and 5 except the red curve displays data from the Geotail spacecraft. The three times of interest in this figure are marked by vertical orange lines at 1456, 1513, and 1528 UT.

3.5. 8 October 2012: IMF By > 0 nT to By < 0 nT

In three of the last four events we were able to observe the asymmetry between the northern and southern equivalent ionospheric currents for two different IMF By directions. In the fourth event we showed the evolution of the equivalent ionospheric currents and current densities shortly after the IMF By changes from positive to negative, but for just the northern hemisphere. In this final event for 8 October 2012 we examine an event with both AMPERE northern and southern hemisphere data and results from the space weather modeling framework (SWMF) during a period when the IMF Bz is strongly negative and the IMF By rotates from a large positive value to a large negative value, which gives us an opportunity to see change in both the northern and southern hemisphere and how well the SWMF can reproduce the interhemispheric asymmetry. See Figure 11, which has the same format as Figure 3. Unfortunately equivalent ionospheric current in the cusp region are not available throughout the event. In Figure 11 we have marked four times: 2206, 2324, 0046, and 0106 UT. During all

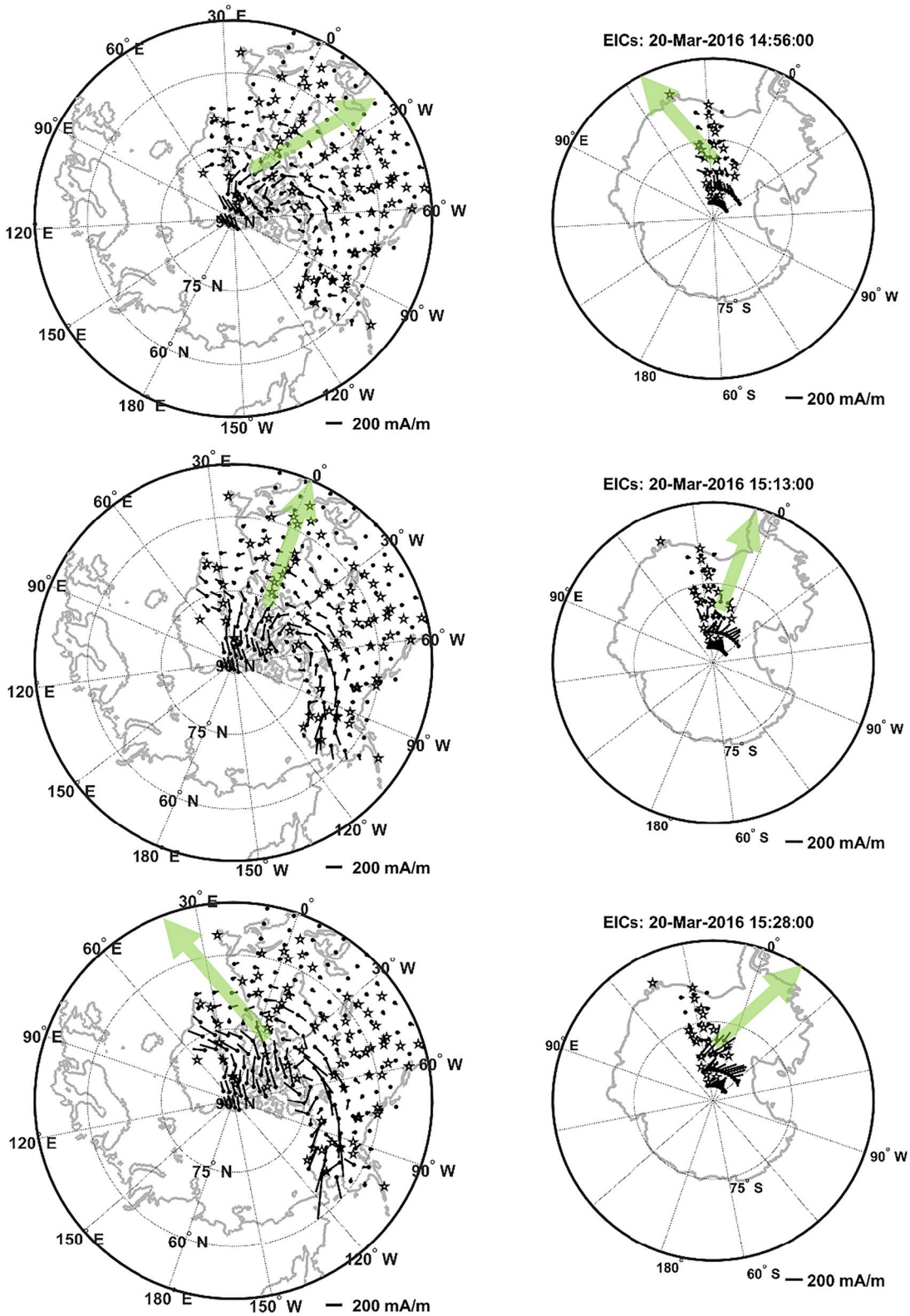

Figure 8. Northern and southern hemisphere equivalent ionospheric currents for 1456, 1513, and 1528 UT on 20 March 2016. The green arrow shows the change in the orientation of the cusp throat region.

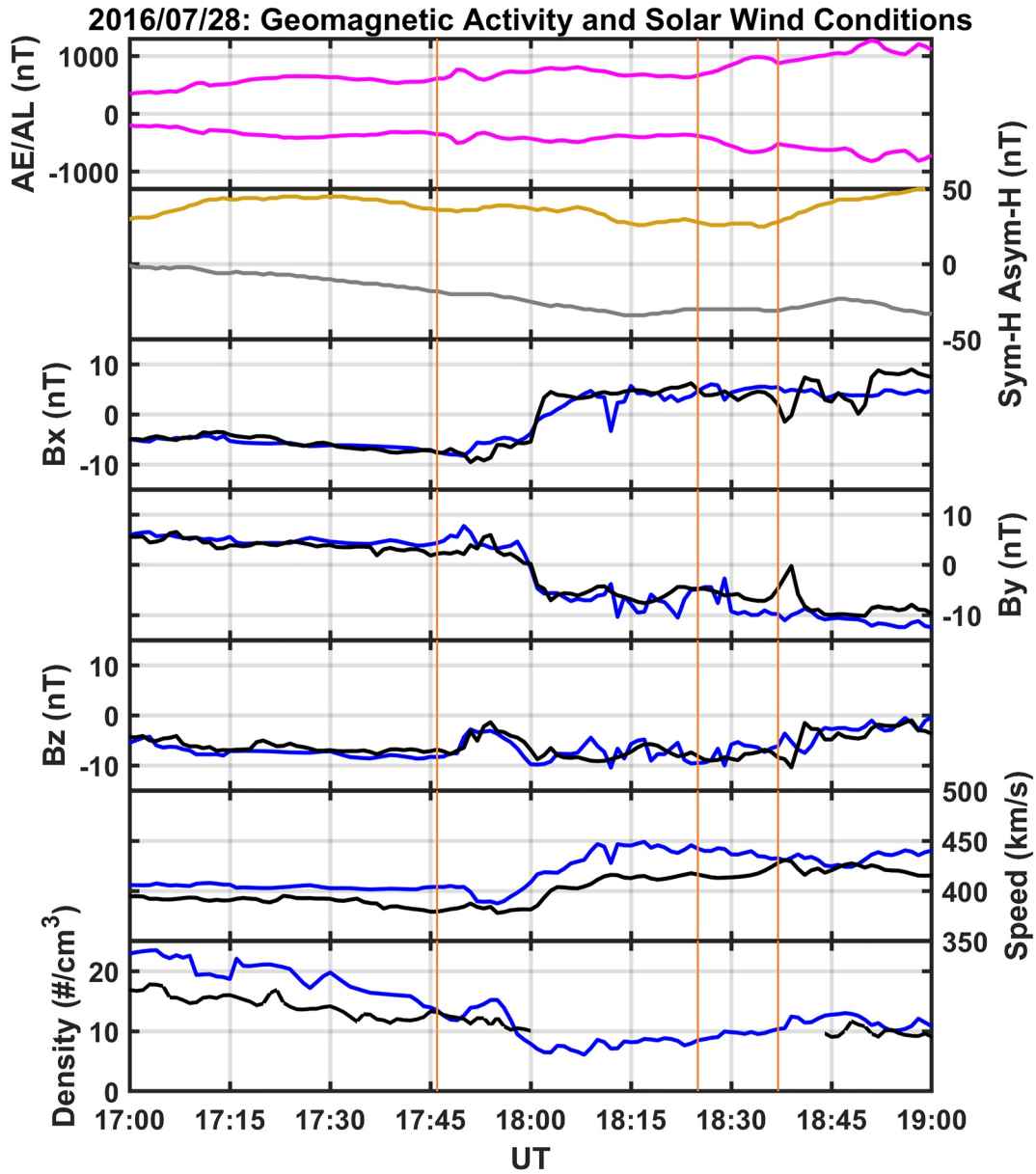

Figure 9. Geomagnetic and solar wind conditions for 28 July 2016. This figure has the same format as Figures 3 and 5. The three times of interest in this figure are marked by vertical orange lines at 1746, 1825, and 1837 UT.

four times the AL index is less than −500 nT and the Sym-H index is just a little larger than −100 nT, which indicates this event occurs during a magnetic storm. In the next three panels of Figure 11 the Bx component is about 0 nT, the By component starts at about +9 nT and then sharply rotates to about −7 nT at about 0020 UT. During the entire interval shown the Bz component is about −14 nT, the solar wind speed is about 400 km/s, and the number density varies between 1.5 and 8 #/cm^3.

In Figure 12 we display the AMPERE current densities in first and third column in both the northern (top row) and southern (bottom row) hemispheres as well as the SWMF current densities in the second and fourth columns for 2206 and 2324 UT. In Figure 13 we show the current densities for AMPERE and SWMF for 0046 and 0106 UT. The color bar for each panel is given on the right side and red indicates upward current and blue indicates downward current. At 2206 and 2324 UT when the IMF By is positive the dayside sector current densities in the AMPERE and SWMF northern hemisphere are identical to the first event examined in this study. See the bottom left of Figure 4. However, the southern hemisphere AMPERE current densities have the same arrangement of

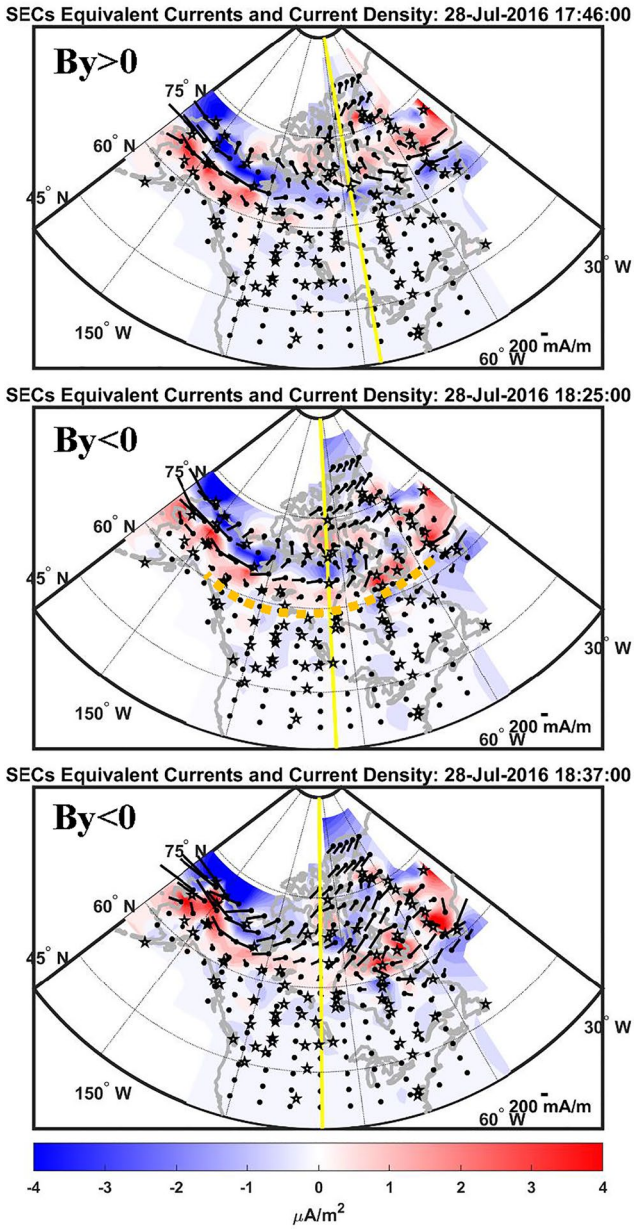

Figure 10. Three sets of SEC maps for 28 July 2016 for three times of interest marked in Figure 9. Each panel shows the combined field-aligned like current densities (red and blue colors) and equivalent currents. The red indicates current upward out of the ionosphere and the blue indicates current into the ionosphere. The yellow vertical bar marks local noon, the key for the equivalent current is given in the lower right corner, and the color bar indicates the current density values at the bottom of the figure.

current as the northern hemisphere and are dissimilar to the southern hemisphere shown in the lower right of Figure 4. In fact, for only a few periods (on the order of about 9 times) after the IMF Bz becomes negative does AMPERE the southern hemisphere current densities resemble the southern hemisphere AMPERE current shown in Figure 4. Furthermore, the southern hemisphere currents stays in the same configuration long after the IMF By switches from positive to negative at about 0020 UT (see the bottom panels of Figure 13) and resembles the southern hemisphere current shown in our second event when IMF By was negative presented in the lower right of Figure 6.

At 2206 UT the southern hemisphere dayside cusp region SWMF current densities are similar to the both the SWMF northern and AMPERE dayside sector current densities. However, at 2324 UT the SWMF dayside cusp region current densities do accurately reproduce the bottom right of Figure 4 for the southern hemisphere for IMF By positive. In addition, there are many more periods (hours) where SWMF more closely resembles the bottom right of Figure 4 than the AMPERE observations.

The northern hemisphere AMPERE current densities begin to resemble the currents shown in the lower left of Figure 6 starting at about 0038 UT approximately 18 min after the IMF By switches from positive to negative at 0020 UT. The northern hemisphere SWMF current densities change a few minutes later at about 0046 UT approximately 26 min after the IMF switches from positive to negative. Both the southern hemisphere AMPERE and SWMF dayside sector current densities resemble the lower right of Figure 6 for By < 0 after 0040 UT without much change for hours after the rotation of the IMF By component.

4. Discussion

We have examined the ionospheric currents for five different events on 17 March 2015, 5 June 2015, 20 March 2016, 28 July 2016, and 8 October 2012. In the first two events both northern and southern hemisphere equivalent ionospheric currents along with AMPERE current densities are available. We found that for 17 March 2015 event when IMF By is positive the cusp throat points towards the dusk in the northern hemisphere and towards the dawn in the southern hemisphere. In the second event the IMF By is negative and the cusp throat points towards the dawn in the northern hemisphere and towards the dusk in the southern hemisphere. In the third event SECs from both the northern and southern hemisphere are available and IMF By rotates from negative to positive. During this rotation the in the northern hemisphere the cusp throat rotated from pointing dawnward to duskward in about 20 min and the opposite rotation occurred in the southern hemisphere. In the fourth event we had only northern hemisphere equivalent ionospheric currents during a period when the IMF By rotates from positive to negative. We observed the equivalent currents in the throat of the cusp rotate from pointing towards the dusk during positive By to pointing dawnward also in about 20 min after the By became negative. In the final event we observed a similar evolution in the AMPERE and SWMF current densities during a period when the IMF rotated from By positive to negative in the northern hemisphere, but a change in the radial currents in the southern hemisphere was nearly nonexistent in the AMPERE current densities and not consistent in the SWMF results.

The equivalent ionospheric currents and AMPERE radial current densities shown in the first two events for IMF By positive and negative (17 March 2015 and 5 June 2016) strongly match the prior models of Cowley et al. (1991), Burch et al. (1985), Reiff and Burch (1985), and Strangeway et al. (2000, 2021). We remind the reader that the equivalent ionospheric currents shown are approximately anti-parallel to the ionospheric flows.

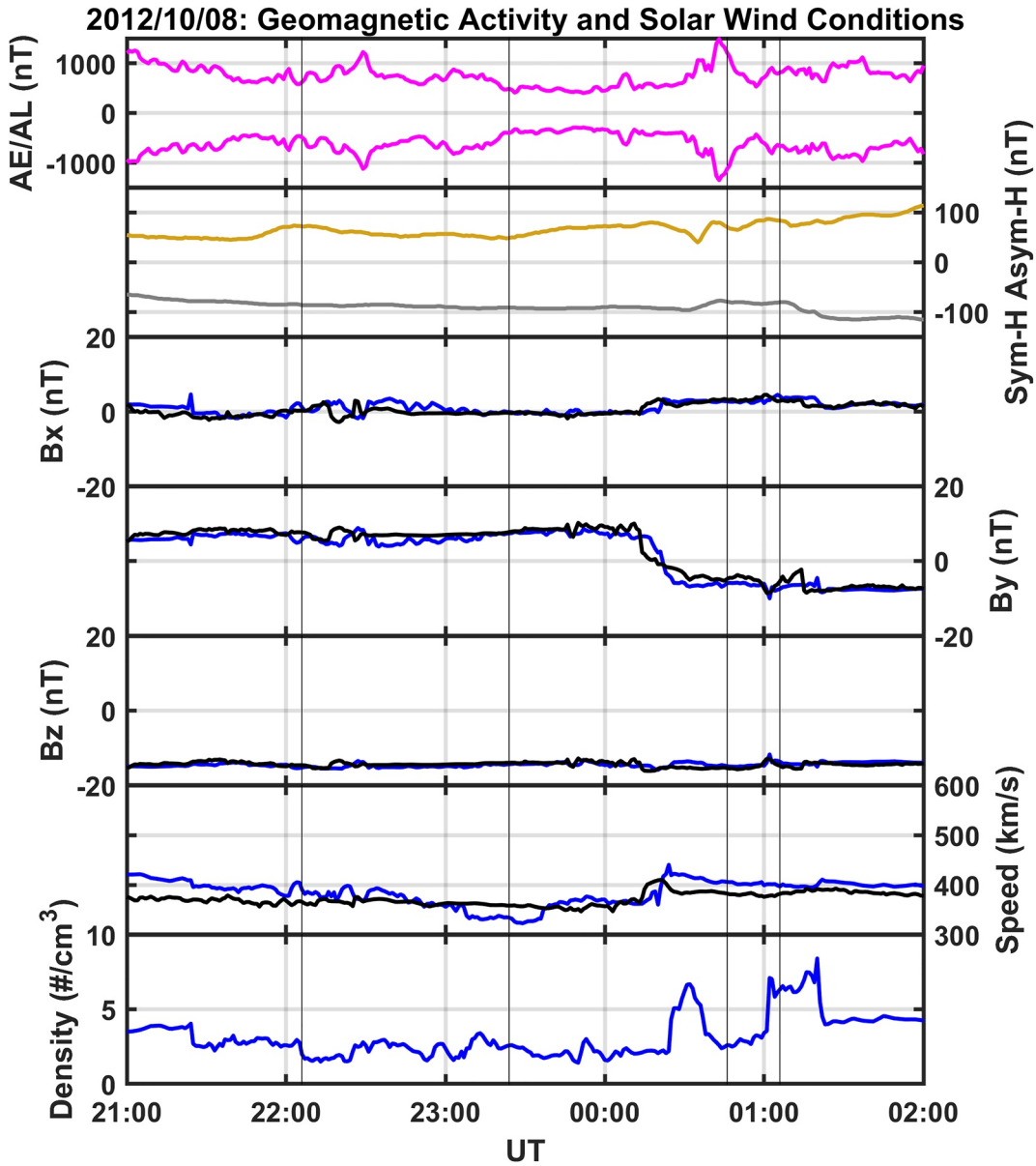

Figure 11. Geomagnetic and solar wind conditions for 8–9 October 2012.

Specifically, for IMF By positive the currents shown in Figure 4 most closely match those of Figure 3a in Cowley et al. (1991). Their Figure 3a shows upward FACs at the highest latitude in the northern hemisphere dayside sector traversing from dusk to nearly dawn, downward FACs equatorward of those all the way from dawn to dusk, then at the equatorward edge again upward currents from dawn to almost noon. This FAC arrangement is similar that shown in the statistical studies of Anderson et al. (2008, 2018) for the northern hemisphere for IMF By positive. Cowley et al. (1991), Figure 3a also shows the flow entering the cusp between the highest latitude upward currents and the adjacent downward current sheet. Strangeway et al. (2000) has a very similar arrangement as that of Cowley et al. (1991) for positive By, but does not provide the direction of the lower latitude region 2 current system. Burch et al. (1985) and Reiff and Burch (1985) display a similar arrangement of cusp FACs and flows to that of Cowley et al. (1991). However, Figure 7a of Burch et al. (1985) suggests that the highest latitude upward FACs may not be one complete sheet from dusk to dawn as we see in our Figure 4 northern hemisphere currents and in Cowley et al. (1991).

Burch et al. (1985) and Reiff and Burch (1985) imply and Strangeway et al. (2021) show that the southern hemisphere radial currents should be the reverse pattern of the northern hemisphere, which is what we observe

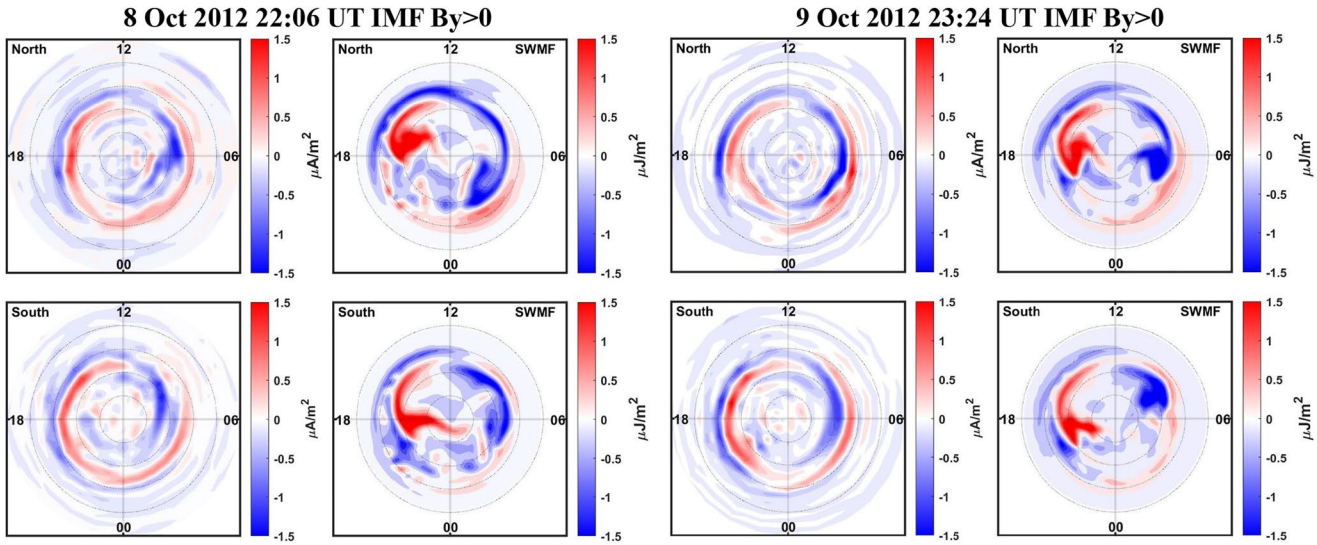

Figure 12. AMPERE and SWMF current densities. In the top row is the current densities for the northern hemisphere and the bottom row is the current densities for the southern hemisphere. The southern hemisphere is shown as a glass earth projection. In the first and third columns are the AMPERE data and the second and fourth columns are the SWMF results. The color bar is given on the right side of each panel and the range for the AMPERE current densities is different from the SWMF data. Blue indicates downward current and red for upward current. The UT time is given in the title of each four sets of currents.

in the 17 March 2015 event. We see that the highest latitude radial AMPERE current is downward from about the dawn to just before dusk, below the highest latitude currents there is an upward current from dusk to dawn, and at the equatorward edge there exists a downward current from dusk until about 11 MLT. This arrange in the southern hemisphere is also observed in Anderson et al. (2018) for IMF By positive. In the southern hemisphere the equivalent currents exit the cusp towards dawn between the highest latitude downward currents and adjacent equatorward upward current sheet.

Specifically, the 5 June 2016 equivalent ionospheric currents and AMPERE radial currents for IMF By negative most resembles Figure 3b of Cowley et al. (1991) for By negative which shows downward field aligned currents at the highest latitude in the northern hemisphere dayside sector traversing from dawn to nearly dusk, upward currents equatorward of those all the way from dawn to dusk, and at the equatorward edge downward currents from dusk to almost noon. This field aligned current arrangement for this event is similar to that shown in the

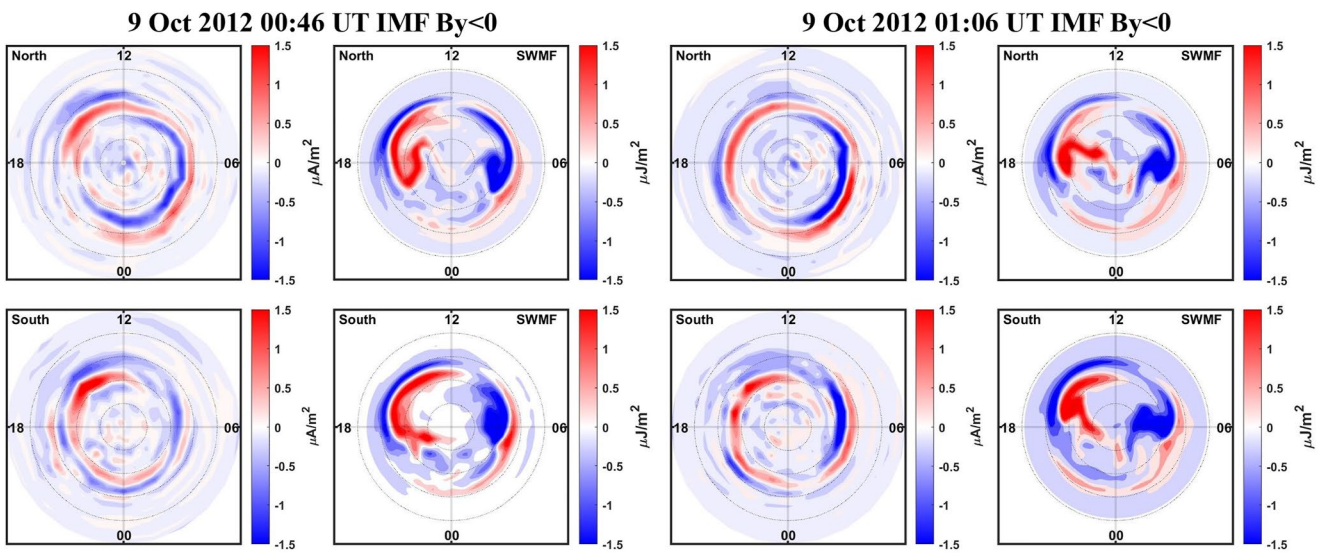

Figure 13. This figure has the same format as Figure 12, but these current densities are for 0046 and 0106 UT.

statistical studies of Anderson et al. (2008, 2018) for IMF By negative. Again, Figure 7b of Burch et al. (1985) suggests that the highest latitude upward FACs may not be one complete sheet from dusk to dawn as we do see in our Figure 6 northern hemisphere currents. Cowley et al. (1991) Figure 3b shows the flow entering the cusp between the highest latitude downward currents and the equatorward upward current sheet from the dawnside which is where our equivalent currents exit the polar cap region. Lastly, we see the opposite arrange in the southern hemisphere compared to the northern hemisphere for this event as Burch et al. (1985), Reiff and Burch (1985), and Strangeway et al. (2021) indicate. The southern hemisphere radial current pattern for 5 June 2016 event matches the bottom panel for the southern hemisphere of Figure 14 of Anderson et al. (2018).

In the 20 March 2016 and 28 July 2016 event we able to observe the evolution in the SEC radial currents and equivalent ionospheric currents as the direction of IMF By rotates from negative to positive and positive to negative, respectively. Furthermore, we were also able to determine the time difference between when the IMF By rotated from negative to positive (20 March 2016) or positive to negative (28 July 2016), which had been propagated to 17 Re out front of the Earth using the Weimer et al. (2003) and Weimer (2004) technique. The observed time difference was about 20 min from when the IMF By was about 0 nT to the new stable configuration of the equivalent currents, but we would expect the travel time of the solar wind from 17 Re to the Earth to be about 4.5 min for a solar wind speed of about 400 km/s specifically for this event. A similar delay time of 5–10 min was determined by Murr and Hughes (2001) using Geotail solar wind data and observation of traveling convection vortices for 7 different events. Ridley et al. (1998) estimated using 65 events that the delay time for ionospheric convection to begin reconfiguring after IMF By and Bz changes reached the magnetopause is about 8.4 ($\pm$8.2) min then an additional 13 min for the convection pattern to completely reconfigure. More recently, Weimer et al. (2010) using solar wind data from 1998 to 2001 and 104 ground magnetometers determined a lag time of about 30 min from the peak of a correlation function comprised of 5 min resolution averaged data. In addition to deriving a time lag, there is a period at about 18:25 UT during the 28 July 2016 event we examined in between the two IMF By extremes when the highest latitude equivalent ionospheric currents are pointing toward the dawn but the equivalent current just equatorward are still pointing toward the dusk. See the middle panel of Figure 10.

For the 8 October 2012 event the IMF By rotated from positive to negative, but equivalent currents in cusp region were not available. Fortunately, the AMPERE radial currents and SWMF model radial currents for both hemispheres are available. The northern hemisphere showed the same orientation in the AMPERE and SWMF radial currents as Cowley et al. (1991), Burch et al. (1985), Reiff and Burch (1985), and our Figure 1 for IMF By positive, however, the southern hemisphere radial currents did not match the prior studies. In fact, for nearly the entire period when IMF By is positive the southern hemisphere AMPERE current densities have the same radial current as the northern hemisphere and resembled the pattern expected for IMF By negative in the southern hemisphere in our Figure 1. Furthermore, the southern hemisphere currents did not significantly change after the IMF By rotates from positive to negative. Similarly, the SWMF cusp region radial currents resemble the IMF By negative FAC current pattern in the southern hemisphere shown in Figure 1 during IMF By positive, but for considerably less time than the AMPERE currents. Specifically, the SWMF southern hemisphere currents spend about 43% of the time in the configuration inconsistent with the IMF By positive given in Figure 1. The reason the southern hemisphere does not consistently match the IMF By positive Figure 1 picture may be related to the values of the IMF By and Bz. In 17 March 2015 event the IMF By was about 20 nT and the Bz about -20 nT, but in the 8 October 2012 event the By was about 8 nT and the Bz about -14 nT. In other words, when the Bz component dominates the By component the cusp throat current patterns may potentially not be in opposite directions in opposite hemispheres and the FAC current pattern would look more like Figure 5s of Anderson et al. (2008). In the prior studies of Cowley et al. (1991), Burch et al. (1985), Reiff and Burch (1985), and displayed in Figure 1, the southward IMF consider was such that $|By| \geq |Bz|$. More research is required for more extreme values of IMF Bz.

The rotation of the By component from positive to negative for the 8 October 2012 event provided another opportunity for determine the time for the cusp currents to evolve from one orientation to another. Here we discuss only the northern hemisphere, which transition from an IMF clock angle of about 151°–205°. The time at which IMF By reached about 0 nT is about 0020 UT and the new configuration of the AMPERE radial currents appeared at about 0038 UT or 18 min after the change in the IMF. In the SWMF model the radial currents took about 26 min to reach the new stable pattern. These values are in general consistent with the approximate 20 min time observed for 20 March 2016 and 28 July 2016 events in the equivalent ionospheric currents, but larger than the 4.5 min for the IMF to propagated from 17 Re to the Earth. We suggest with the limited number of cases available here that

the reconfiguration of the dayside currents is about 20 min, however, the accuracy of the propagation from the ACE and Wind spacecraft from the L1 point to 17 Re on the XGSM line is unclear. Cameron and Jackel (2016) suggested that the approximate uncertainty for the Weimer propagation technique is on the order of 5.5 min. However, this value would depend on the tilt of the IMF phase plane orientations and the distance of the spacecraft off the X-GSM axis.

As discussed in the introduction, the location of the cusp throat region does not just indicate the location of the convective flow into the polar cap, it also potentially indicates the shape of the dayside reconnection line. Crooker (1979) and Trattner et al. (2007a, 2007b, 2012, 2021) showed that when IMF By component is positive or negative the reconnection line can become twisted and the throat of cusp may no longer open towards magnetic noon. Generally, when throat of cusp opens towards the dusk in the northern hemisphere for IMF By positive Crooker (1979), Trattner et al. (2007a, 2007b, 2012, 2021), and Tenfjord et al. (2015) demonstrated antiparallel reconnection occurs at a higher latitude on the duskside of the magnetosphere above the magnetic equatorial plane and at lower latitudes below the magnetic equatorial on the dawnside of the magnetosphere. Specifically, the 17 March 2015 event has a clock angle of about 135° and the reconnection line should resemble the white curve (the antiparallel reconnection line) in the lower left panel of Figure 7 of Trattner et al. (2007b). For IMF By negative the opposite arrangement of the antiparallel reconnection line occurs (Crooker, 1979; Trattner et al., 2007a, 2007b, 2012, 2021). Specifically, the 5 June 2016 event has a clock angle of about 225° and the reconnection line should resemble the white curve (the antiparallel reconnection line) in the right panel of Figure 9 of Trattner et al. (2007b). Furthermore, during the 28 July 2016 event the antiparallel reconnection line should traverse across the surface of the magnetosphere when the IMF By and Bz rotate from a clock angle of about 145°–227°, which is similar to the large clock angle changes of the other two events just discussed (i.e., 8 October 2012: from about 151° to 205° and 20 March 2016 from about 215° to 160°).

5. Conclusion

In this study we have examined the equivalent ionosphere current pattern, AMPERE radial current pattern, and SWMF current patterns for five events with IMF By positive and negative. We summarize the main results of the study here.

1. The equivalent ionospheric current pattern and AMPERE radial current pattern for the northern hemisphere dayside matches the model proposed in Cowley et al. (1991), which has the throat of the cusp pointing duskward for IMF By positive and dawnward for By negative.
2. The ionospheric dayside current pattern for the dayside in the southern hemisphere is opposite that of the northern hemisphere. That is to say, the throat of the cusp points dawnward for IMF By positive and duskward for By negative.
3. The AMPERE southern hemisphere radial currents during the extreme 8 October storm did not resemble the expected current pattern and appeared to be more similar to the northern hemisphere.
4. In general the SWMF reproduces the northern hemisphere 8 October 2012 results, but not as clearly in the southern hemisphere.
5. We found that the time it takes for the ionospheric currents to adjust after the propagated IMF rotates from positive to negative is on the order of 18–20 min.
6. The interhemispheric asymmetry observed in the cusp throat suggests that reconnection line varies with IMF By in accordance with Crooker (1979) and Trattner et al. (2007a, 2007b, 2012, 2021).

The SECS technique applied for the first time to magnetically conjugate northern and southern hemisphere regions to produce instantaneous equivalent ionospheric current maps represent a value added product from the raw magnetometer database. These maps can be used for interhemispheric studies, contextual interpretation, as well as help with our understanding of magnetosphere-ionosphere coupling mechanisms. At this time sufficient ground magnetometer data in the southern hemisphere is available to produce 2 years' worth (2015–2016) of ionospheric current maps that could be used for both events studies and statistical studies.

Data Availability Statement

SECS data for North America and Greenland from 2007 through 2019 are available at http://vmo.igpp.ucla.edu/data1/SECS/. AMPERE data are available at https://ampere.jhuapl.edu/. ACE and Wind IMF and solar wind data are available at CDAWeb https://cdaweb.gsfc.nasa.gov/. AE, AL, Asym-H, and Sym-H indices are available

at https://wdc.kugi.kyoto-u.ac.jp/. The AGO/SPA/MCM data can be found at antarcticgeospace.njit.edu. The British Antarctic survey magnetometer data is available at https://data.bas.ac.uk/full-record.php?id=GB/NERC/BAS/PDC/00263, CARISMA magnetometer data is available at http://data.carisma.ca/FGM/1Hz/. Finally the Virginia Tech magnetometer data can be found at http://themis.ssl.berkeley.edu/data/themis/thg/l2/mag/.

Acknowledgments
J.M. Weygand would like to acknowledge NSF GEO-NERC award number 2027190, NASA contract 80GSFC17C0018, NASA award number 80NSSC18K1220, and NASA HSR award number 80NSSC18K1227. R.J. Strangeway, D. Welling, and J.M. Weygand would like to acknowledge NASA DRIVE/UTA award number 80675. We thank the many different groups operating magnetometer arrays for providing data for this study including: We thank the AALPIP magnetometer team at mist.nianet.org for supplying Antarctica magnetometer data. The work at New Jersey Institute of Technology was supported by NASA Grant 80NSSC21K0132 and NSF Grant OPP-1744861. The fluxgate magnetometer projects at South Pole and AGO stations are supported by NSF Grants OPP-1643700 and PLR-1443507, respectively, managed by the New Jersey Institute of Technology. We thank Andrew J. Gerrard for making these data available. We thank Mervyn P. Freeman for making the British Antarctic Survey magnetometer data available. We thank Brian J. Anderson, the AMPERE team, and the AMPERE Science Data Center for providing data products derived from the Iridium Communications constellation, enabled by support from the National Science Foundation. The THEMIS UCLA magnetometer network (Ground-based Imager and Magnetometer Network for Auroral Studies) is funded through NSF Grant AGS-1004736. The authors thank I.R. Mann, D.K. Milling and the rest of the CARISMA team for data. CARISMA is operated by the University of Alberta, funded by the Canadian Space Agency. The Canadian Magnetic Observatory Network (CANMON) is maintained and operated by the Geological Survey of Canada—http://gsc.nrcan.gc.ca/geomag. The Magnetometer Array for Cusp and Cleft Studies (MACCS) array is supported by US National Science Foundation Grant ATM-0827903 at Augsburg University and M. J. Engebretson, D. Murr, and E.S. Steinmetz. The McMAC Project is sponsored by the Magnetospheric Physics Program of National Science Foundation through Grant AGS-0245139 and was maintained by Dr. Peter Chi. The Falcon magnetometers were maintained by United States Air Force Academy (USAFA) and Peter Chi. We would like to thank the DTU magnetometer team. The Solar and Terrestrial Physics (STEP) magnetometer file storage is at Department of Earth and Planetary Physics, University of Tokyo and maintained by Dr. Kanji Hayashi. Finally, the United States Geological Survey (USGS) Geomagnetism Program.

References

Amm, O., & Viljanen, A. (1999). Ionospheric disturbance magnetic field continuation from the ground to the ionosphere using spherical elementary current systems. *Earth Planets and Space*, *51*(6), 431–440. https://doi.org/10.1186/bf03352247

Anderson, B. J., Korth, H., Waters, C. L., Green, D. L., & Stauning, P. (2008). Statistical Birkeland current distributions from magnetic field observations by the Iridium constellation. *Annales de Geophysique*, *26*(3), 671–687. https://doi.org/10.5194/angeo-26-671-2008

Anderson, B. J., Olson, C. N., Korth, H., Barnes, R. J., Waters, C. L., & Vines, S. K. (2018). Temporal and spatial development of global Birkeland currents. *Journal of Geophysical Research: Space Physics*, *123*(6), 4785–4808. https://doi.org/10.1029/2018JA025254

Anderson, B. J., Takahashi, K., & Toth, B. A. (2000). Sensing global Birkeland currents with Iridium® engineering magnetometer data. *Geophysical Research Letters*, *27*(24), 4045–4048. https://doi.org/10.1029/2000GL000094

Benkevitch, L. V., Koustov, A. V., Liang, J., & Waterman, J. F. (2006). Comparison of the magnetic equivalent convection direction and ionospheric convection observed by the SuperDARN radars. *Annales Geophysicae*, *24*(11), 2981–2990. https://doi.org/10.5194/angeo-24-2981-2006

Burch, J. L., Reiff, P. H., Menietti, J. D., Heelis, R. A., Hanson, W. B., Shawhan, S. D., et al. (1985). IMF By-dependent plasma flow and Birkeland currents in the dayside magnetosphere: 1. Dynamics explorer observations. *Journal of Geophysical Research*, *90*(A2), 1577–1593. https://doi.org/10.1029/ja090ia02p01577

Cameron, T., & Jackel, B. (2016). Quantitative evaluation of solar wind time-shifting methods. *Space Weather*, *14*(11), 973–981. https://doi.org/10.1002/2016SW001451

Chi, P. J., Engebretson, M. J., Moldwin, M. B., Russell, C. T., Mann, I. R., Hairston, M. R., et al. (2013). Sounding of the plasmasphere by mid-continent MAgnetoseismic Chain (McMAC) magnetometers. *Journal of Geophysical Research: Space Physics*, *118*(6), 3077–3086. https://doi.org/10.1002/jgra.50274

Clauer, C. R., Kim, H., Deshpande, K., Xu, Z., Weimer, D., Musko, S., et al. (2014). An autonomous adaptive low-power instrument platform (AAL-PIP) for remote high-latitude geospace data collection. *Geoscientific Instrumentation, Methods and Data Systems*, *3*(2), 211–227. https://doi.org/10.5194/gi-3-211-2014

Cowley, S. W. H. (1981). Magnetospheric asymmetries associated with the Y-component of the IMF. *Planetary and Space Science*, *29*(1), 79–96. https://doi.org/10.1016/0032-0633(81)90141-0

Cowley, S. W. H., Morelli, J. P., & Lockwood, M. (1991). Dependence of convective flows and particle precipitation in the high-latitude dayside ionosphere on the X and Y components of the interplanetary magnetic field. *Journal of Geophysical Research*, *96*(A4), 5557–5564. https://doi.org/10.1029/90ja02063

Cowley, S. W. H., & Owen, C. J. (1989). A simple illustrative model of open flux tube motion over the dayside magnetopause. *Planetary and Space Science*, *37*(11), 1461–1475. https://doi.org/10.1016/0032-0633(89)90116-5

Crooker, N. U. (1979). Dayside merging and cusp geometry. *Journal of Geophysical Research*, *84*(A3), 951–959. https://doi.org/10.1029/ja084ia03p00951

de La Beaujardiere, O., Watermann, J., Newell, P., & Rich, F. (1993). Relationship between Birkeland current regions, particle precipitation, and electric fields. *Journal of Geophysical Research*, *98*(A5), 7711–7720. https://doi.org/10.1029/92ja02005

Dungey, J. W. (1961). Interplanetary magnetic field and auroral zones. *Physical Review Letters*, *6*(2), 47–48. https://doi.org/10.1103/physrevlett.6.47

Engebretson, M. J., Hughes, W. J., Alford, J. L., Zesta, E., Cahill, L. J., Jr., Arnoldy, R. L., & Reeves, G. D. (1995). Magnetometer array for cusp and Cleft studies observations of the spatial extent of broadband ULF magnetic pulsations at cusp/cleft latitudes. *Journal of Geophysical Research*, *100*(A10), 19371. https://doi.org/10.1029/95ja00768

Mann, I. R., Milling, D. K., Rae, I. J., Ozeke, L. G., Kale, A., Kale, Z. C., et al. (2008). The upgraded CARISMA magnetometer array in the THEMIS era. *Space Science Reviews*, *141*(1–4), 413–451. https://doi.org/10.1007/s11214-008-9457-6

Matzka, J. (2016). Geomagnetic observatories. *Journal of Large-Scale Research Facilities*, *2*, A83. https://doi.org/10.17815/jlsrf-2-136

Melville, R., Stillinger, A., Gerrard, A., & Weatherwax, A. (2014). Sustainable energy at the 100 W level for scientific sites on the Antarctic Plateau: Lessons learned from the polar experiment network for geospace upper atmosphere investigations-automatic geophysical observatory project. *Review of Scientific Instruments*, *85*(4), 45117. https://doi.org/10.1063/1.4871555

Mende, S. B., Rachelson, W., Sterling, R., Frey, H. U., Harris, S. E., McBride, S., et al. (2009). Observations of Earth space by self-powered stations in Antarctica. *Review of Scientific Instruments*, *80*(12), 124501. https://doi.org/10.1063/1.3262506

Murr, D. L., & Hughes, W. J. (2001). Reconfiguration timescales of ionospheric convection. *Geophysical Research Letters*, *28*(11), 2145–2148. https://doi.org/10.1029/2000gl012765

Reiff, P. H., & Burch, J. L. (1985). IMF By-dependent plasma flow and Birkeland currents in the dayside magnetosphere: 2. A global model for northward and southward IMF. *Journal of Geophysical Research*, *90*(A2), 1595–1609. https://doi.org/10.1029/ja090ia02p01595

Ridley, A. J., Lu, G., Clauer, C. R., & Papitashvili, V. O. (1998). A statistical study of the ionospheric convection response to changing interplanetary magnetic field conditions using the assimilative mapping of ionospheric electrodynamics technique. *Journal of Geophysical Research*, *103*(A3), 4023–4039. https://doi.org/10.1029/97ja03328

Russell, C. T., Chi, P. J., Dearborn, D. J., Ge, Y. S., Kuo-Tiong, B., Means, J. D., et al. (2008). THEMIS ground-based magnetometers. *Space Science Reviews*, *141*(1–4), 389–412. https://doi.org/10.1007/s11214-008-9337-0

Strangeway, R. J., Russell, C. T., Carlson, C. W., McFadden, J. P., Ergun, E. R., Temerin, M., et al. (2000). Cusp field-aligned currents and ion outflows. *Journal of Geophysical Research*, *105*(A9), 21129–21141. https://doi.org/10.1029/2000ja900032

Strangeway, R. J., Weygand, J. M., Anderson, B. J., Raeder, J., Runov, A., Lopez, R. E., & Welling, D. T. (2021). Dependence of the cusp-region Birkeland current structure on the interplanetary magnetic field orientation as observed during October 8-9, 2012. In *Fall meeting 2020*. American Geophysical Union. abstract #SA025-03.

Tenfjord, P., Østgaard, N., Snekvik, K., Laundal, K. M., Reistad, J. P., Haaland, S., & Milan, S. E. (2015). How the IMF By induces a By component in the closed magnetosphere and how it leads to asymmetric currents and convection patterns in the two hemispheres. *Journal of Geophysical Research: Space Physics*, *120*(11), 9368–9384. https://doi.org/10.1002/2015JA021579

Thomas, E. G., & Shepherd, S. G. (2018). Statistical patterns of ionospheric convection derived from mid-latitude, high-latitude, and polar SuperDARN HF radar observations. *Journal of Geophysical Research: Space Physics*, *123*(4), 3196–3216. https://doi.org/10.1002/2018JA025280

Trattner, K. J., Mulcock, J. S., Petrinec, S. M., & Fuselier, S. A. (2007a). Location of the reconnection line at the magnetopause during southward IMF conditions. *Geophysical Research Letters*, *34*(3), L03108. https://doi.org/10.1029/2006gl028397

Trattner, K. J., Mulcock, J. S., Petrinec, S. M., & Fuselier, S. A. (2007b). Probing the boundary between antiparallel and component reconnection during southward interplanetary magnetic field conditions. *Journal of Geophysical Research*, *112*(A8), A08210. https://doi.org/10.1029/2007ja012270

Trattner, K. J., Petrinec, S. M., & Fuselier, S. A. (2021). The location of magnetic reconnection at Earth's magnetopause. *Space Science Reviews*, *217*(3), 1–47. https://doi.org/10.1007/s11214-021-00817-8

Trattner, K. J., Petrinec, S. M., Fuselier, S. A., & Phan, T. D. (2012). The location of reconnection at the magnetopause: Testing the maximum magnetic shear model with THEMIS observations. *Journal of Geophysical Research*, *117*(A1), A01201. https://doi.org/10.1029/2011ja016959

Waters, C. L., Anderson, B. J., & Liou, K. (2001). Estimation of global field aligned currents using the Iridium® system magnetometer data. *Geophysical Research Letters*, *28*(11), 2165–2168. https://doi.org/10.1029/2000GL012725

Weimer, D. R. (2004). Predicting interplanetary magnetic field (IMF) propagation delay times using the minimum variance technique. *Journal of Geophysical Research*, *109*(A12), 1026.

Weimer, D. R., Clauer, C. R., Engebretson, M. J., Hansen, T. L., Gleisner, H., Mann, I., & Yumoto, K. (2010). Statistical maps of geomagnetic perturbations as a function of the interplanetary magnetic field. *Journal of Geophysical Research*, *115*(A10), A10320. https://doi.org/10.1029/2010JA015540

Weimer, D. R., Ober, D. M., Maynard, N. C., Collier, M. R., McComas, D. J., Ness, N. F., et al. (2003). Predicting interplanetary magnetic field (IMF) propagation delay times using the minimum variance technique. *Journal of Geophysical Research*, *108*(A1), 1026. https://doi.org/10.1029/2002JA009405

Wesche, C., Weller, R., König-Lango, G., Fromm, T., Eckstaller, A., Nixdorf, U., & Kohlberg, E. (2016). Neumayer III and Kohnen station in Antarctica operated by the Alfred Wegener Institute. *Journal of Large-Scale Research Facilities*, *2*(A85). https://doi.org/10.17815/jlsrf-2-152

Weygand, J. M. (2009a). Equivalent ionospheric currents (EICs) derived using the spherical elementary current systems (SECS) technique at 10 s resolution in geographic coordinates. *UCLA*. https://doi.org/10.21978/P8D62B

Weygand, J. M. (2009b). Spherical elementary current (SEC) amplitudes derived using the spherical elementary current systems (SECS) technique at 10 s resolution in geographic coordinates. *UCLA*. https://doi.org/10.21978/P8PP8X

Weygand, J. M., Amm, O., Angelopoulos, V., Milan, S. E., Grocott, A., Gleisner, H., & Stolle, C. (2012). Comparison between SuperDARN flow vectors and equivalent ionospheric currents from ground magnetometer arrays. *Journal of Geophysical Research*, *117*(A5), A05325. https://doi.org/10.1029/2011JA017407

Weygand, J. M., Amm, O., Viljanen, A., Angelopoulos, V., Murr, D., Engebretson, M. J., et al. (2011). Application and validation of the spherical elementary currents systems technique for deriving ionospheric equivalent currents with the North American and Greenland ground magnetometer arrays. *Journal of Geophysical Research*, *116*(A3), A03305. https://doi.org/10.1029/2010JA016177

Weygand, J. M., & Wing, S. (2016). Comparison of DMSP and SECS region-1 and region-2 ionospheric current boundary. *Journal of Atmospheric and Solar-Terrestrial Physics*, *143*, 8–13. https://doi.org/10.1016/j.jastp.2016.03.002

Xu, Z., Hartinger, M. D., Clauer, C. R., Peek, T., & Behlke, R. (2017). A comparison of the ground magnetic responses during the 2013 and 2015 St. Patrick's Day geomagnetic storms. *Journal of Geophysical Research: Space Physics*, *122*(4), 4023–4036. https://doi.org/10.1002/2016JA023338